A Unique Solution of Planet and Star Parameters from an Extrasolar Planet Transit Light Curve

2003 ApJ 585 1038

(http://iopscience.iop.org/0004-637X/585/2/1038)

The Astrophysical Journal, 585:1038–1055, 2003 March 10

A UNIQUE SOLUTION OF PLANET AND STAR PARAMETERS FROM AN EXTRASOLAR PLANET TRANSIT LIGHT CURVE

S. Seager[1,2] and G. Mallén-Ornelas[3,4]

Received 2002 June 11; accepted 2002 November 13

ABSTRACT

There is a unique solution of the planet and star parameters from a planet transit light curve with two or more transits if the planet has a circular orbit and the light curve is observed in a bandpass where limb darkening is negligible. The existence of this unique solution is very useful for current planet transit surveys for several reasons. First, there is an analytic solution that allows a quick parameter estimate, in particular of R_p. Second, the stellar density can be uniquely derived from the transit light curve alone. The stellar density can then be used to immediately rule out a giant star (and hence a much larger than planetary companion) and can also be used to put an upper limit on the stellar and planet radius even considering slightly evolved stars. Third, the presence of an additional fully blended star that contaminates an eclipsing system to mimic a planet transit can be largely ruled out from the transit light curve given a spectral type for the central star. Fourth, the period can be estimated from a single-transit light curve and a measured spectral type. All of these applications can be used to select the best planet transit candidates for mass determination by radial velocity follow-up. To use these applications in practice, the photometric precision and time sampling of the light curve must be high (better than 0.005 mag precision and 5 minute time sampling for a two-transit light curve).

Subject headings: binaries: eclipsing — planetary systems — techniques: photometric

1. INTRODUCTION

Planet transit searches for close-in extrasolar giant planets (planets with orbital semimajor axes $\sim$0.05 AU) promise to be the next big step forward for extrasolar planet detection and characterization. Every transiting planet discovered will have a measured radius. A radius is necessary to constrain the planet evolution and migration history and also provides constraints on planet composition and atmosphere through evolutionary models. The importance of measured radii for a number of close-in giant planets cannot be overstated. Recent theoretical studies (Guillot & Showman 2002) of planet evolution in close proximity to a parent star are unable to match the radius from the preferred model with the measured radius of the transiting planet HD 209458b to 20%–30%. This implies that there are atmospheric or interior physical processes taking place that are not currently known. Many more planetary radii will be needed to help fully resolve this discrepancy.

In addition to radius, the absolute mass of transiting planets will be determined from combined transit and radial velocity measurements. Note, however, that for the current state of theoretical models a precise radius measurement (as described above) is more important than a precise mass. Minimum masses (from $M \sin i$), or even just a census of approximate planetary masses, are sufficient constraints for the current state of planetary formation and migration theories (with the exception of studies of planetary dynamics of known extrasolar planet systems).

There are many other benefits of planet transit searches. Planets can be discovered around distant stars and in a variety of environments. Because of their special geometry, many follow-up observations of transiting planets are possible, such as atmosphere transmission spectroscopy (note the first extrasolar planet atmosphere detection by Charbonneau et al. 2002), search for moons and rings (Brown et al. 2001), and detection of oblateness and the corresponding constraint on rotation rate (Seager & Hui 2002). Note that the photometric signatures of moons, rings, planetary oblateness, and atmospheric refraction are much smaller than the transit signature itself and so will have a negligible effect on basic parameters derived from a planet transit light curve.

Although no planet candidates discovered by the transit method have yet been confirmed by mass measurements, many searches are currently ongoing. The OGLE-III planet search (Udalski et al. 2002a, 2002b) has observed numerous high-precision transit light curves from objects with small radii, including several potential planets. The EXPLORE search (Mallén-Ornelas et al. 2003) has four potential planet candidates based on both photometric light curves and follow-up radial velocity measurements (Yee et al. 2003; Mallén-Ornelas et al. 2002; G. Mallén-Ornelas et al. 2003, in preparation). The Vulcan planet search (Borucki et al. 2001) has some published results on transit candidates that, with radial velocity measurements, were determined to be eclipsing binary stars (Jenkins, Caldwell, & Borucki 2002).

[1] Institute for Advanced Study, Einstein Drive, Princeton, NJ 08540.

[2] Current address: Department of Terrestrial Magnetism, Carnegie Institution of Washington, 5241 Broad Branch Road NW, Washington, DC 20015; seager@dtm.ciw.edu.

[3] Princeton University Observatory, Peyton Hall, Princeton, NJ 08544-0001; and Departamento de Astronomía y Astrofísica, Pontificia Universidad Católica de Chile, Casilla 306, Santiago 22, Chile.

[4] Current address: Harvard-Smithsonian Center for Astrophysics, 60 Garden Street, MS 15, Cambridge, MA 02138; gmalleno@cfa.harvard.edu.

Follow-up mass determination by radial velocity measurements is needed for planet transit candidates because late M dwarfs ($M \geq 80\ M_J$), brown dwarfs ($13\ M_J < M < 80\ M_J$), and gas giant planets ($M \leq 13\ M_J$) are all of similar sizes. This is due to a coincidental balance between Coulomb forces (which cause $R \sim M^{1/3}$) and electron degeneracy pressure (which causes $R \sim M^{-1/3}$). A high yield of confirmed planets from a list of planet candidates considered for mass follow-up is important, especially for planet searches with faint stars (e.g., fainter than 13th magnitude), which require relatively long exposures on 8 m class telescopes (e.g., 20–30 minutes per star for a single radial velocity measurement). Hence, understanding the transit light curves before follow-up can be crucial for any survey with a large number of planet transit candidates.

An analytical solution is always worthwhile to understand the general properties of a given physical system in an intuitive form. This is the case even when numerical fits are in practice the best way to determine the system parameters. In the case of a planet transit light curve we found that there is a unique solution for the five parameters stellar mass M_*, stellar radius R_*, companion radius R_p, orbital semimajor axis a, and orbital inclination i, under some important assumptions. This unique solution has several interesting applications (especially when the photometric precision and time sampling are high), including selection of the best planet candidates for follow-up mass measurements. Selection of the best candidates is especially important if the tendency for planets with small orbital semimajor axes to have low mass (Zucker & Mazeh 2002)—and hence low radial velocity amplitudes—is generally true. In this case, on average, more effort will be needed to detect the planet mass via radial velocity variations of the parent star since the primary star's radial velocity amplitude scales linearly with planet mass.

The unique solution to a light curve with two or more transits was first mentioned in Mallén-Ornelas et al. (2003), where an approximate set of equations and a short description were presented. Sackett (1999) briefly touches on the unique solution by outlining parameter derivation with a known stellar spectral type, including a mention of period determination from a single transit. Schneider & Chevreton (1990) have earlier addressed period determination from a single transit of a star with a known spectral type. Some textbooks (e.g., Kopal 1979) analytically describe eclipsing binary stars, but to our knowledge we present for the first time the general equations and the unique solution of the planet-star parameters for an extrasolar planet transit. Moreover, we show for the first time that the stellar density can be obtained from the planet transit light curve alone together with Kepler's third law. The results of this paper are intended to aid in selection of the best planet transit candidates for mass follow-up measurements. Much can be learned from the transit light curve alone. Moreover, complementing transit light curves with spectral types is even more helpful for candidate selection.

We begin this paper by describing the assumptions necessary to determine the unique solution in § 2. In § 3 we present both the general set of equations that describe a planet transit light curve and their analytic solution. We discuss the errors in the parameters, and hence the limiting photometric precision and time sampling needed for the applications outlined in this paper, in § 4. In § 5 we present four interesting applications that are made possible by the unique solution to the planet transit light curve. The complications of limb darkening are discussed in § 6. Section 7 concludes this paper with a summary.

2. ASSUMPTIONS

The unique determination of the stellar mass M_*, stellar radius R_*, companion radius R_p, orbital semimajor axis a, and orbital inclination i from a light curve with two or more eclipses requires the following assumptions:

1. The planet orbit is circular.
2. $M_p \ll M_*$ and the companion is dark compared to the central star.
3. The stellar mass-radius relation is known.
4. The light comes from a single star, rather than from two or more blended stars.

The unique determination also requires the light curve to fulfill the following conditions:

1. The eclipses have flat bottoms, which implies that the companion is fully superimposed on the central star's disk.
2. The period can be derived from the light curve (e.g., the two observed eclipses are consecutive).

The first three assumptions are all reasonable for current extrasolar planet transit searches. Circular orbits are expected for short-period planets as a result of their short tidal circularization timescale, and all but one of the currently known short-period planets (<4.3 days) have eccentricities consistent with zero.[5] All current ground-based transit searches are searching for or expecting to find mostly short-period planets, which have the highest geometric probability to show transits. The stellar mass-radius relation is reasonably well known for each separate class of stars (e.g., main sequence), and as we show later, the mass-radius relation is not needed for a derivation of all parameters. The only assumption that has a significant chance of being wrong is the absence of contaminating light from an additional, fully blended star. An eclipsing binary system could be so contaminated by a third star, either a physical companion or a chance alignment of a foreground or background star along the line of sight. This "blended" situation and its possible identification are discussed in § 5. The required conditions listed above are also all reasonable. Flat-bottomed transits will appear in a bandpass where limb darkening is weak (within the limits of realistic time sampling and observational noise), such as I band. Several transit surveys are using I band, including OGLE-III (Udalski et al. 2002a, 2002b), EXPLORE (Mallén-Ornelas et al. 2003), and STEPPS, and follow-up measurements for other surveys could be taken in I band or in even a redder color in order to exploit the unique solution discussed in this paper (see § 6 for a discussion of limb darkening). For the rest of the paper we will work under the assumptions and conditions listed above, unless otherwise stated.

[5] See the Extrasolar Planets Encyclopaedia, available at http://cfa-www.harvard.edu/planets.

3. THE EQUATIONS AND SOLUTION FOR A LIGHT CURVE WITH TWO OR MORE TRANSITS

3.1. *The General System of Equations*

There are five equations that completely describe the planet transit light curve. The first three equations (eqs. [1]–[3]) describe the geometry of the transit in terms of transit depth, transit shape, and transit duration (see Fig. 1). For a planet transit light curve that is due to two spheres passing in front of each other, the geometry is relatively straightforward (see Sackett 1999 for a derivation of the transit duration eq. [3]). Here we parameterize the transit shape by both t_T, the total transit duration (first to fourth contact), and t_F, the duration of the transit completely inside ingress and egress (second to third contact). The three geometrical equations that describe the transit light curve depend on four observables: the period P, the transit depth ΔF, t_F, and t_T. See Figure 1 for an illustrative definition of ΔF, t_F, and t_T. In addition to the three geometrical equations, there are two physical equations (eqs. [4] and [5]), Kepler's third law and the stellar mass-radius relation. It is these physical equations that break the degeneracy of the mathematical description of two spheres passing in front of each other, by setting a physical scale. It is this physical scale, together with the geometrical description, that allows the unique solution.

The equations are as follows: the transit depth, ΔF, with F defined as the total observed flux,

$$\Delta F \equiv \frac{F_{\text{no transit}} - F_{\text{transit}}}{F_{\text{no transit}}} = \left(\frac{R_p}{R_*}\right)^2 ; \tag{1}$$

the transit shape, described by the ratio of the duration of the "flat part" of the transit (t_F) to the total transit duration (t_T),

$$\frac{\sin(t_F\pi/P)}{\sin(t_T\pi/P)} = \frac{\left\{\left[1-\left(R_p/R_*\right)\right]^2-\left[(a/R_*)\cos i\right]^2\right\}^{1/2}}{\left\{\left[1+\left(R_p/R_*\right)\right]^2-\left[(a/R_*)\cos i\right]^2\right\}^{1/2}} ; \tag{2}$$

the total transit duration,

$$t_T = \frac{P}{\pi}\arcsin\left(\frac{R_*}{a}\left\{\frac{\left[1+\left(R_p/R_*\right)\right]^2-\left[(a/R_*)\cos i\right]^2}{1-\cos^2 i}\right\}^{1/2}\right) ; \tag{3}$$

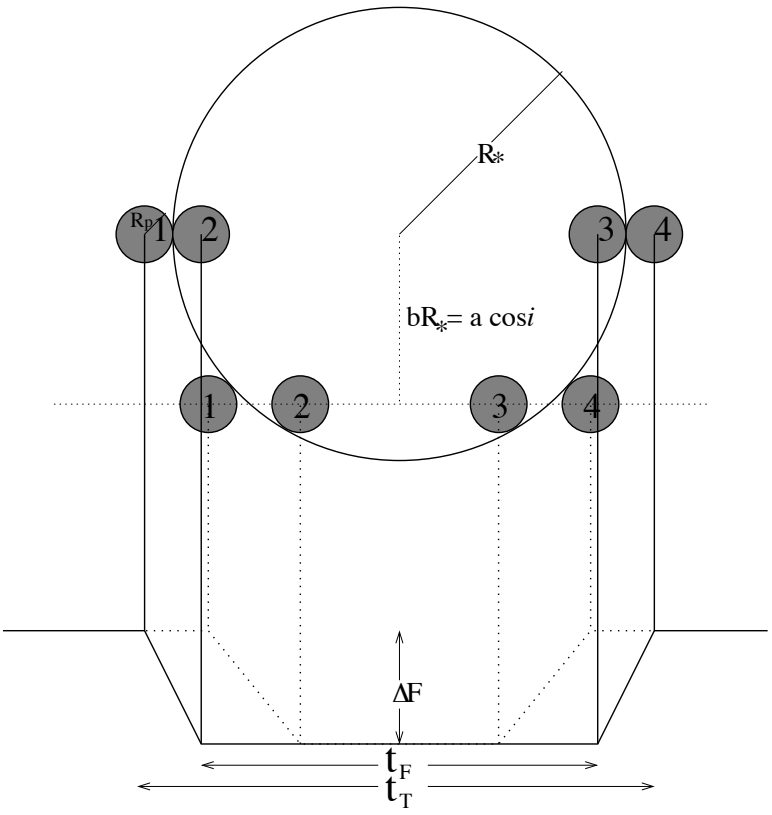

FIG. 1.—Definition of transit light-curve observables. Two schematic light curves are shown on the bottom (*solid and dotted lines*), and the corresponding geometry of the star and planet is shown on the top. Indicated on the solid light curve are the transit depth ΔF, the total transit duration t_T, and the transit duration between ingress and egress t_F (i.e., the "flat part" of the transit light curve when the planet is fully superimposed on the parent star). First, second, third, and fourth contacts are noted for a planet moving from left to right. Also defined are R_*, R_p, and impact parameter b corresponding to orbital inclination i. Different impact parameters b (or different i) will result in different transit shapes, as shown by the transits corresponding to the solid and dotted lines.

Kepler's third law, assuming a circular orbit, where G is the universal gravitational constant and M_p the planet mass,

$$P^2 = \frac{4\pi^2 a^3}{G(M_* + M_p)} \; ; \tag{4}$$

and the stellar mass-radius relation,

$$R_* = kM_*^x \; , \tag{5}$$

where k is a constant coefficient for each stellar sequence (main sequence, giants, etc.) and x describes the power law of the sequence (e.g., $x \simeq 0.8$ for F–K main-sequence stars; Cox 2000).

3.2. *Analytical Solution*

3.2.1. *Four Parameters Derivable from Observables*

We ultimately wish to solve for the five unknown parameters M_*, R_*, a, i, and R_p from the five equations above. It is first useful to note that four combinations of physical parameters can be found directly from the observables (ΔF, t_T, t_F, and P) using only the first four equations in § 3.1 (the three transit geometry equations and Kepler's third law with $M_p \ll M_*$); this avoids any uncertainty from the stellar mass-radius relation.

The four combinations of parameters are as follows: the planet-star radius ratio, which trivially follows from equation (1),

$$\frac{R_p}{R_*} = \sqrt{\Delta F} \; ; \tag{6}$$

the impact parameter b, defined as the projected distance between the planet and star centers during midtransit in units of R_* (see Fig. 1), and which can be derived directly from the transit shape equation (2), together with equation (6),

$$b \equiv \frac{a}{R_*}\cos i = \left\{ \frac{\left(1 - \sqrt{\Delta F}\right)^2 - \left[\sin^2(t_F\pi/P)/\sin^2(t_T\pi/P)\right]\left(1 + \sqrt{\Delta F}\right)^2}{1 - \left[\sin^2(t_F\pi/P)/\sin^2(t_T\pi/P)\right]} \right\}^{1/2} \; ; \tag{7}$$

the ratio a/R_*, which can be derived directly from the transit duration equation (3),

$$\frac{a}{R_*} = \left\{ \frac{\left(1 + \sqrt{\Delta F}\right)^2 - b^2\left[1 - \sin^2(t_T\pi/P)\right]}{\sin^2(t_T\pi/P)} \right\}^{1/2} \; ; \tag{8}$$

and the stellar density ρ_*, which can be derived from the above equation for a/R_* and Kepler's third law with $M_p \ll M_*$ (eq. [4]),

$$\rho_* \equiv \frac{M_*}{R_*^3} = \left(\frac{4\pi^2}{P^2 G}\right)\left\{ \frac{\left(1 + \sqrt{\Delta F}\right)^2 - b^2\left[1 - \sin^2(t_T\pi/P)\right]}{\sin^2(t_T\pi/P)} \right\}^{3/2} \; . \tag{9}$$

The parameters b and a/R_* are dimensionless. The density can be written in units of $\rho_\odot$ by substituting $4\pi^2/G = 365.25^2/215^3$ day^2 $M_\odot/R_\odot^3$.

It is interesting to consider the geometrical and physical origin of these combinations of parameters. The impact parameter b depends almost entirely on the transit shape (parameterized by t_F/t_T) and the ratio of planet and star sizes [$(\Delta F)^{1/2}$]. To a lesser extent b depends mildly on the period (see § 3.3.2). The term a/R_* is the ratio of orbital semimajor axis to planet radius; to first order it is related to the ratio of transit duration to total period. The term a/R_* is also dependent on the impact parameter b and planet-star size ratio because these parameters affect the transit duration. The stellar density, ρ_*, comes from Kepler's third law and the transit duration t_T; Kepler's third law describes how much mass is enclosed inside the planet's orbit, and the stellar radius is described by the transit duration with a physical scale set by Kepler's third law. Again, ρ_* is also dependent on the impact parameter b and the planet-star size ratio because these parameters affect the transit duration.

3.2.2. *The Five Physical Parameters*

The five physical parameters R_*, M_*, i, a, and R_p can be derived from the above solution for R_p/R_*, b, a/R_*, and ρ_* by using one additional equation: the stellar mass-radius relation (eq. [5]). To derive M_*, consider equation (9) together with the stellar mass-radius relation in the form $\rho_*/\rho_\odot \equiv M_*/M_\odot(R_*/R_\odot)^{-3} = (M_*/M_\odot)^{1-3x}1/k^3$:

$$\frac{M_*}{M_\odot} = \left(k^3\frac{\rho_*}{\rho_\odot}\right)^{1/(1-3x)} \; . \tag{10}$$

The stellar radius can be derived from the stellar mass by the stellar mass-radius relation, or from the density directly,

$$\frac{R_*}{R_\odot} = k\left(\frac{M_*}{M_\odot}\right)^x = \left(k^{1/x}\frac{\rho_*}{\rho_\odot}\right)^{x/(1-3x)} \; ; \tag{11}$$

the orbital radius a can be derived from M_* and from Kepler's third law with $M_p \ll M_*$,

$$a = \left(\frac{P^2 G M_*}{4\pi^2}\right)^{1/3} ; \tag{12}$$

based on the definition of impact parameter (eq. [7]), the orbital inclination is

$$i = \cos^{-1}\left(b\frac{R_*}{a}\right) ; \tag{13}$$

and most importantly, the planetary radius is

$$\frac{R_p}{R_\odot} = \frac{R_*}{R_\odot}\sqrt{\Delta F} = \left(k^{1/x}\frac{\rho_*}{\rho_\odot}\right)^{x/(1-3x)}\sqrt{\Delta F} . \tag{14}$$

For main-sequence stars $k = 1$ and $x \approx 0.8$, in which case $R_p/R_\odot = (\rho_*/\rho_\odot)^{-0.57}(\Delta F)^{1/2}$.

3.3. *The Simplified Set of Equations and Their Solution*

The equations and five-parameter solution take on a simpler form under the assumption $R_* \ll a$. This assumption is equivalent to $t_T\pi/P \ll 1$ (from eq. [8]) and has as its consequence $\cos i \ll 1$ (from eq. [13]). Systems we are interested in generally have $t_T\pi/P < 0.15$ and likely $t_T\pi/P \lesssim 0.1$ (or $R_*/a \gtrsim \frac{1}{8}$). Mathematically this assumption allows $\arcsin x \approx x$ and $\sin x \approx x$. Under this approximation, $\sin(t_F\pi/P)/\sin(t_T\pi/P) \approx t_F/t_T$. A comparison of these two terms is shown in Figure 2*a*; for cases of interest the terms agree to better than 4% and much better in most cases. Under the approximation $t_T\pi/P \ll 1$, a second term of interest arises, $1 - \sin^2(t_T\pi/P) \approx 1$. A comparison of this term as a function of $t_T\pi/P$ (Fig. 2*b*) shows agreement to better than 2.5% for cases of interest. The simplified solution will allow us to explore useful applications analytically in § 5.

3.3.1. *The Simplified Equations*

Under the approximations $t_T\pi/P \ll 1$, the transit shape (eq. [2]) with $\sin x \approx x$ becomes independent of P,

$$\left(\frac{t_F}{t_T}\right)^2 = \frac{(1 - R_p/R_*)^2 - [(a/R_*)\cos i]^2}{(1 + R_p/R_*)^2 - [(a/R_*)\cos i]^2} , \tag{15}$$

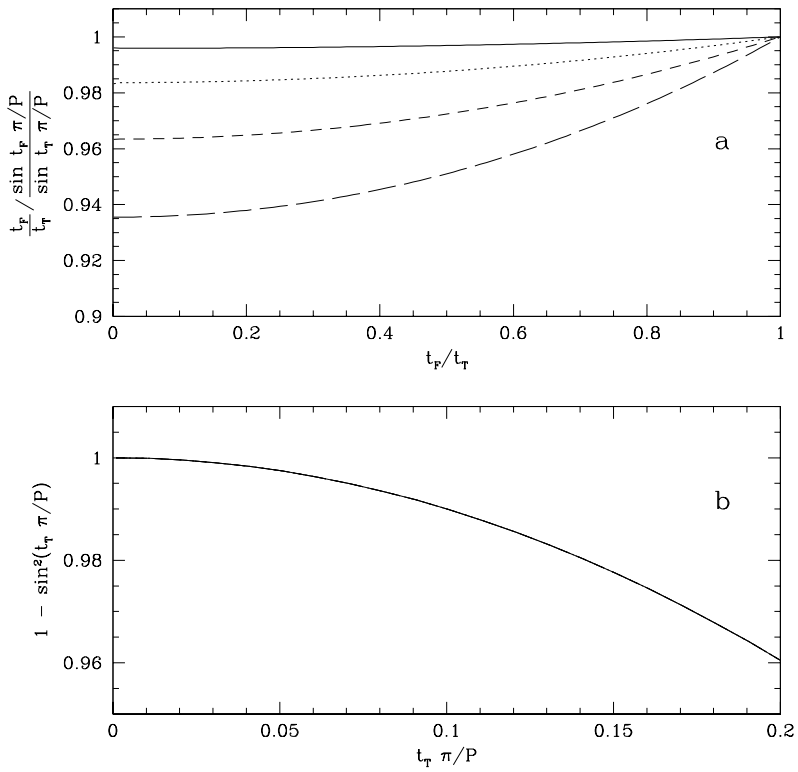

FIG. 2.—Validity of the approximation $t_T P/\pi \ll 1$ (or equivalently $R_* \ll a$). This approximation allows $\sin(t_T P/\pi) \approx t_T P/\pi$. (*a*) Term of interest $\sin(t_F\pi/P)/\sin(t_T\pi/P)$ is reasonably well approximated by t_F/t_T. The different lines correspond to different values of $t_T\pi/P$: 0.05 (*solid line*), 0.1 (*dotted line*), 0.15 (*short-dashed line*), and 0.2 (*long-dashed line*). (*b*) Term of interest $1 - \sin^2(t_T\pi/P)$ compared to its value, 1, under the approximation $t_T P/\pi \ll 1$. The short-period planet transit systems of interest will have $t_T\pi/P < 0.15$ and usually $t_T\pi/P \lesssim 0.1$.

and the total transit duration (eq. [3]) with $\cos i \ll 1$ becomes

$$t_T = \frac{PR_*}{\pi a}\sqrt{\left(1+\frac{R_p}{R_*}\right)^2 - \left(\frac{a}{R_*}\cos i\right)^2}\ . \tag{16}$$

The other three equations for transit depth (eq. [1]), Kepler's third law (eq. [4]), and the mass-radius relation (eq. [5]) remain the same as in the exact solution. Note that by substituting $b = (a/R_*)\cos i$ and $(\Delta F)^{1/2} = R_p/R_*$ the above equations take a very simple form.

3.3.2. *The Simplified Analytical Solution*

The solution to the simplified equations is more useful than the exact solution for considering the general properties of light curves because P either cancels out of the solution or is a simple factor that can cancel out in parameter ratios. The impact parameter b (eq. [7]), under the approximation $t_T\pi/P \ll 1$, becomes

$$b = \left[\frac{\left(1-\sqrt{\Delta F}\right)^2 - (t_F/t_T)^2\left(1+\sqrt{\Delta F}\right)^2}{1-(t_F/t_T)^2}\right]^{1/2}\ , \tag{17}$$

the ratio a/R_* (eq. [8]) becomes

$$\frac{a}{R_*} = \frac{2P}{\pi}\frac{\Delta F^{1/4}}{\left(t_T^2 - t_F^2\right)^{1/2}}\ , \tag{18}$$

and the stellar density ρ_* (eq. [9]) becomes

$$\rho_* = \frac{32}{G\pi}P\frac{\Delta F^{3/4}}{\left(t_T^2 - t_F^2\right)^{3/2}}\ . \tag{19}$$

Note that ρ_* can be written in units of $\rho_\odot$ for P, t_F, and t_T in days, with the first factor on the right-hand side of equation (19) written as $32/G\pi = 3.46 \times 10^{-3}$ day^2 $M_\odot/R_\odot^3$. The equation for R_p/R_* (eq. [6]) clearly remains the same as in the nonsimplified case. The stellar mass, stellar radius, orbital semimajor axis, orbital inclination, and planet radius can be derived as before with equations (10)–(14).

4. ERRORS

In principle, the unique solution of ρ_* and of the parameters M_*, R_*, i, a, and R_p provides a powerful tool for understanding the transit light curve and more importantly for selecting the best transit candidates for radial velocity follow-up. In practice, the usefulness of the unique solution is limited by errors caused by the limited photometric precision and time sampling of real data. The errors in the star-planet parameters are very non-Gaussian and often correlated, so a simulation is necessary in order to estimate errors. To compute the errors as a function of photometric precision and time sampling, we generated 1000 simulated two-transit light curves with added Gaussian noise in the photometry for each of several combinations of photometric precision (σ) and time sampling (δt). We considered values of σ of 0.0025, 0.005, 0.01, and 0.015 mag and values of δt of 2.7, 6, and 12 minutes. Note that the shortest time sampling and highest photometric precision are reachable by current transit surveys (e.g., Mallén-Ornelas et al. 2003). We then fitted the simulated transits for period, phase, depth, impact parameter, and stellar density with a χ^2 minimization fit. Additionally we solved for the planet radius using the main-sequence stellar mass-radius relation with $x = 0.8$. For specificity we chose a star-planet model of $P = 3.0$ days, $M_* = M_\odot$, $R_* = R_\odot$, and $\Delta F = 2\%$ (hence $R_p = 0.14\ R_\odot = 1.45\ R_J$). Limb darkening was not included (see § 6). We considered models with two different impact parameters ($b = 0.2$, which corresponds to $t_F/t_T = 0.74$, and $b = 0.7$, which corresponds to $t_F/t_T = 0.55$) because the errors are very sensitive to impact parameter of the input transit. Although for specificity we have focused on a single model (with two different impact parameters), for the purpose of error estimates changing t_T (by a change in P, ΔF, and a; see eq. [3] or eq. [16]) is equivalent to a linear change in time sampling, and changing ΔF (by a change in R_p or R_*; see eq. [1]) is equivalent to a linear change in photometric precision. Thus, errors in parameters from other models can be considered using the same computational results. Here we focus on the two most interesting parameters, ρ_*, which can tell us if the star is on or close to the main sequence, and R_p, an obvious quantity of interest for selecting the best planet candidates.

The errors in ρ_* and R_p are dominated by errors in the impact parameter b, which we discuss first. Figure 3 shows that for a given ΔF there is a one-to-one correspondence between the impact parameter b and the transit shape as parameterized by t_F/t_T; this one-to-one correspondence is one of the reasons for the existence of the unique solution. For "box-shaped" transits with large values of t_F/t_T, a small change in t_F/t_T can result in a very large change in b, making it difficult to derive b accurately from box-shaped transit light curves. This is not the case for transits with small t_F/t_T (i.e., with very long ingress/egress times), where b changes little even for a relatively large change in t_F/t_T. In the case of noisy data, b will be underestimated as a result of asymmetric errors resulting from the nonlinear relation between b and t_F/t_T. An underestimate in b corresponds to an overestimate in ρ_* and an underestimate in R_* and R_p.

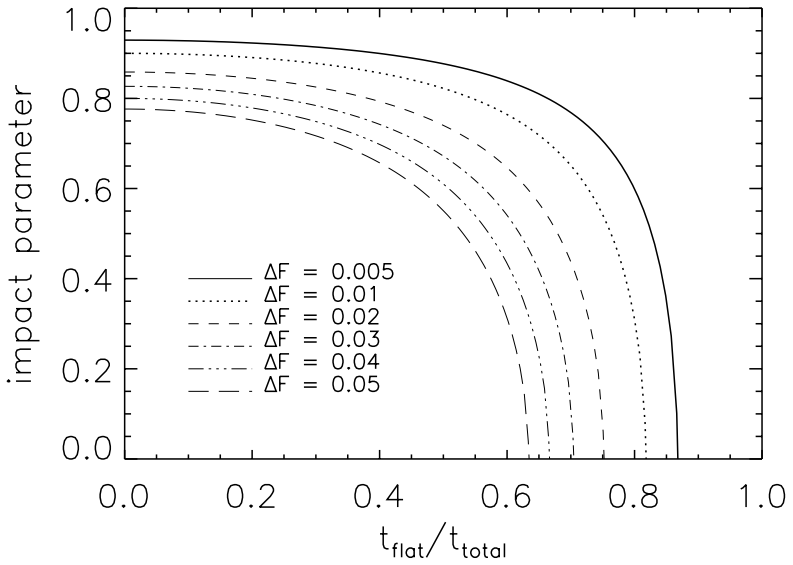

FIG. 3.—One-to-one correspondence between the transit shape as parameterized by t_F/t_T and the impact parameter b for a given transit depth ΔF (eq. [17]). This one-to-one correspondence is one of the elements that makes the unique solution to the transit light curve possible. Transits with a given ΔF can only fall along a given b-t_F/t_T curve, and for a given ΔF there is a maximum b and a corresponding minimum t_F/t_T. For large values of t_F/t_T (box-shaped transits), a small change in t_F/t_T can result in a large change in b, making it difficult to derive b accurately from the transit light curve. This effect also causes an underestimate in b when the transit light curve is noisy because a symmetric error in t_F/t_T causes a very asymmetric error in b.

Figures 4, 5, and 6 show the errors in b and the fractional errors in ρ_* and R_p for the simulations on the specific transit model described above. Results for $b = 0.2$ are shown in the left-hand panels, and results for $b = 0.7$ are shown in the right-hand panels. The top and middle panels, respectively, show the rms and the median of the difference between the fit results and the input parameter (e.g., the rms and median of $\{b_{\mathrm{fit},i} - b_{\mathrm{input}}\}$, where the $b_{\mathrm{fit},i}$ are the fit results from each of the 1000 simulated noisy light curves and b_{input} is the actual value used to create those light curves). The bottom panels show histograms of the fit results for each combination of photometric precision and time sampling. The vertical dotted lines indicate the correct value for the parameter in question (0.2 or 0.7 for b, and 0 in the case of fractional deviation for ρ_* and R_p). From the median deviation plots and the histograms themselves, notice the severe systematic underestimate of b and the resulting overestimate of ρ_* and R_p for cases with $\sigma \gtrsim 0.005$ mag and $b = 0.7$. The rms fractional errors in ρ_* are 10% for $b = 0.2$ and 20% for $b = 0.7$ for a photometric precision of 0.0025 and a time sampling of 2.7 minutes. For this photometric precision and time sampling, the errors in R_p are less than 10% (neglecting uncertainty in the stellar mass-radius relation). The errors in R_p are $\lesssim 40\%$ for time samplings $\lesssim 6$ minutes and photometric precision $\lesssim 0.005$. These errors are quoted for the two-transit light-curve model used here, and as described above, errors for models with different parameters (with the exception of changes in b) can be derived by scaling δt and σ together with t_T and ΔF. Note that multiple low–time-sampled transit light curves can be folded for higher effective time sampling and are useful as long as the photometric precision is high enough. A main point of these error simulations is that the transit shape must be well defined by high photometric precision and high time sampling because most star-planet parameters depend on transit shape. Specifically, a limiting factor is time sampling of ingress and egress and their start and end times to determine transit shape.

The errors for different combinations of photometric precision (σ) and time sampling (δt) are related because the total signal-to-noise ratio per transit is based on both σ and δt. In particular, the total number of photons per transit goes roughly as

$$N_{\mathrm{photons\ per\ transit}} \sim \left(\frac{t_T}{\delta t}\right)\left(\frac{1}{\sigma^2}\right). \tag{20}$$

It is interesting to note that our simulations show that the same error distribution will result from δt and σ combinations that give the same total number of photons per transit. For example, compare the errors for a given δt and σ with those for $4\delta t$ and $\sigma/2$. This can be seen in Figure 6, where the same errors and error distribution result for $\delta t = 12$ minutes, $\sigma = 0.0025$ mag and for $\delta t = 2.7$ minutes, $\sigma = 0.005$ mag. Taking this into account, an optimal strategy of time sampling and exposure time can be chosen for a given mirror size and detector read time. Note that, in practice, $\delta t \ll t_T$ is required in order to reach reasonable errors in the derived parameters.

5. APPLICATIONS

The existence of a unique solution to a planet transit light curve has several applications. The first application is an analytic solution for planet-star parameters by using the equations in § 3.2.2 with the values from § 3.2.1 or § 3.3.2. This analytical solution is useful for a quick parameter estimate. In this section we use the simplified analytic solution (§ 3.3) to explore the usefulness of four additional applications.

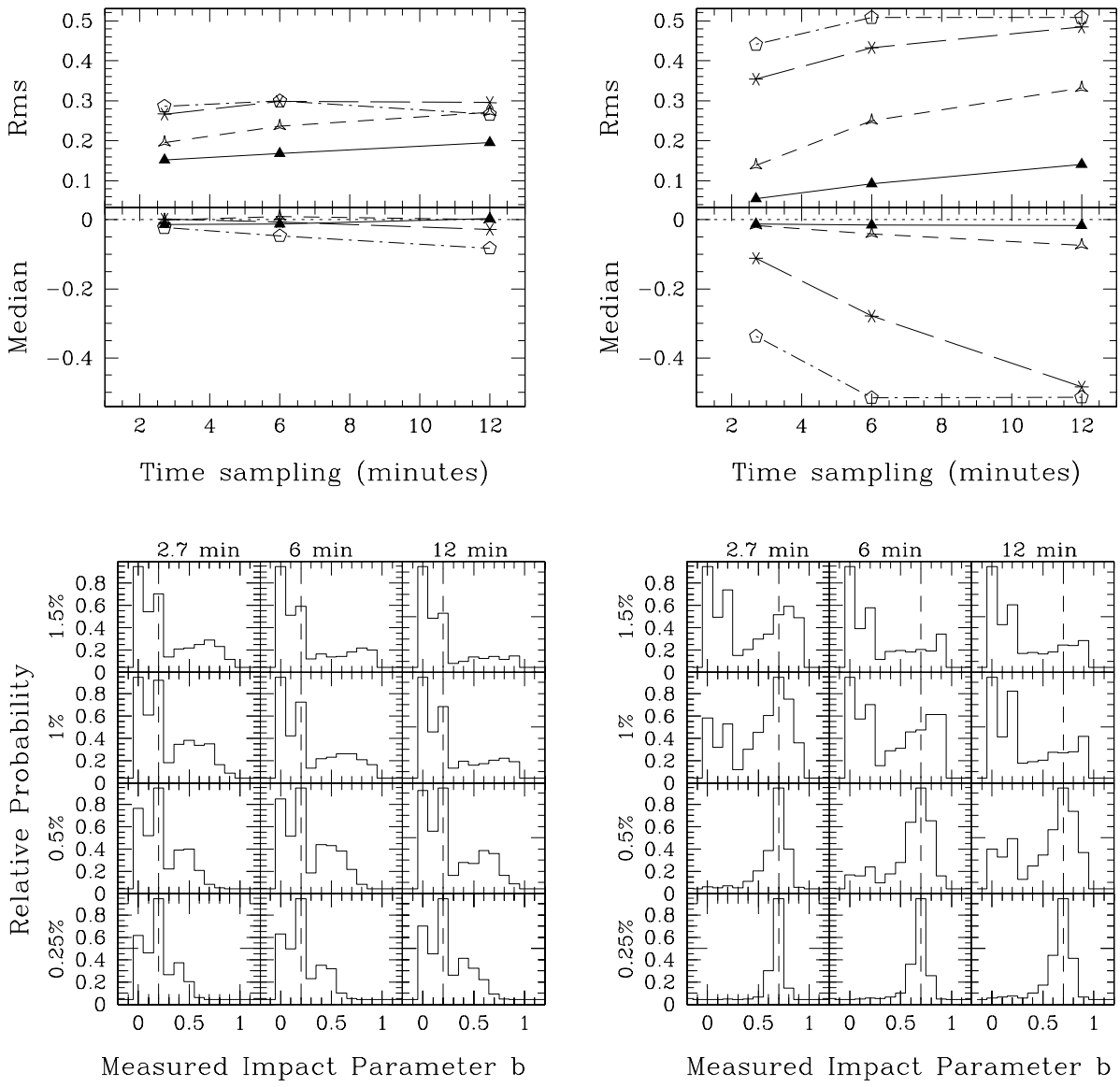

FIG. 4.—Errors in the derived impact parameter for the model $P = 3.0$ days, $M_* = M_\odot$, $R_* = R_\odot$, $\Delta F = 2\%$ (hence $R_p = 0.14\ R_\odot = 1.45\ R_J$), and no limb darkening. The left-hand panels are for $b = 0.2$, and the right-hand panels for $b = 0.7$. For each combination of photometric precision $\sigma = 0.0025$, 0.005, 0.01, and 0.015 mag and time sampling $\delta t = 2.7$, 6, and 12 minutes, 1000 noisy model transits were created and fitted. The top panels show the rms of the difference between the measured and input b. The middle panels show the median of the difference between the measured and input b (an indication of systematic errors in the fits). The different curves are for different photometric precision $\sigma = 0.015$ (*pentagons*), 0.01 (*asterisks*), 0.005 (*open triangles*), and 0.0025 (*filled triangles*), and time sampling is shown in the x-axis. Notice the systematic underestimate of b, especially evident for the $b = 0.7$ models with large σ and δt. The bottom panels show normalized histograms of the fit values for b for the different combinations of δt (increasing from left to right) and σ (increasing from bottom to top). The dotted line in each subpanel indicates the input value for b. The figure shows that very high time sampling and high photometric precision are needed for a reasonably accurate fit ($\lesssim$10%–20% errors). When either the time sampling or photometric precision is very low, the value of b is consistently underestimated by the χ^2 fits (see text and Fig. 3). The panels in this figure can be used to estimate errors in parameters from different models (for the same b) by considering that changing t_T causes a linear change in time sampling and changing ΔF causes a linear change in error in photometric precision. Note the trade-off in σ vs. δt, where combinations with the same $\sigma^2 \delta t$ have nearly identical error distributions.

5.1. *Measuring Stellar Density Directly from the Transit Light Curve*

The density $\rho_* = M_* R_*^{-3}$, as described analytically in equations (9) and (19), is directly measurable from the light-curve observables (ΔF, t_T, t_F, and P), together with Kepler's third law. A measured density makes it possible to immediately distinguish between a main-sequence star and a giant star from the transit light curve alone (i.e., without color data or spectra). Knowing the stellar size to first order immediately is useful for an estimate of R_p from the depth of the transit (eq. [14]). For example, eclipses of $\Delta F = 1\%$ for a giant star would be caused by a stellar companion, not a planetary companion. Figure 7 shows the density as a function of spectral type. A density measurement would give a position on the y-axis only. As shown by the box in Figure 7, F0 V–M0 V stars occupy a unique region of stellar density parameter space. Hence, a density measurement can tell us that a given star is in the vicinity of main-sequence stars. The main-sequence stellar spectral type can be estimated for a given ρ_* by using the mass-radius relation for main-sequence stars.

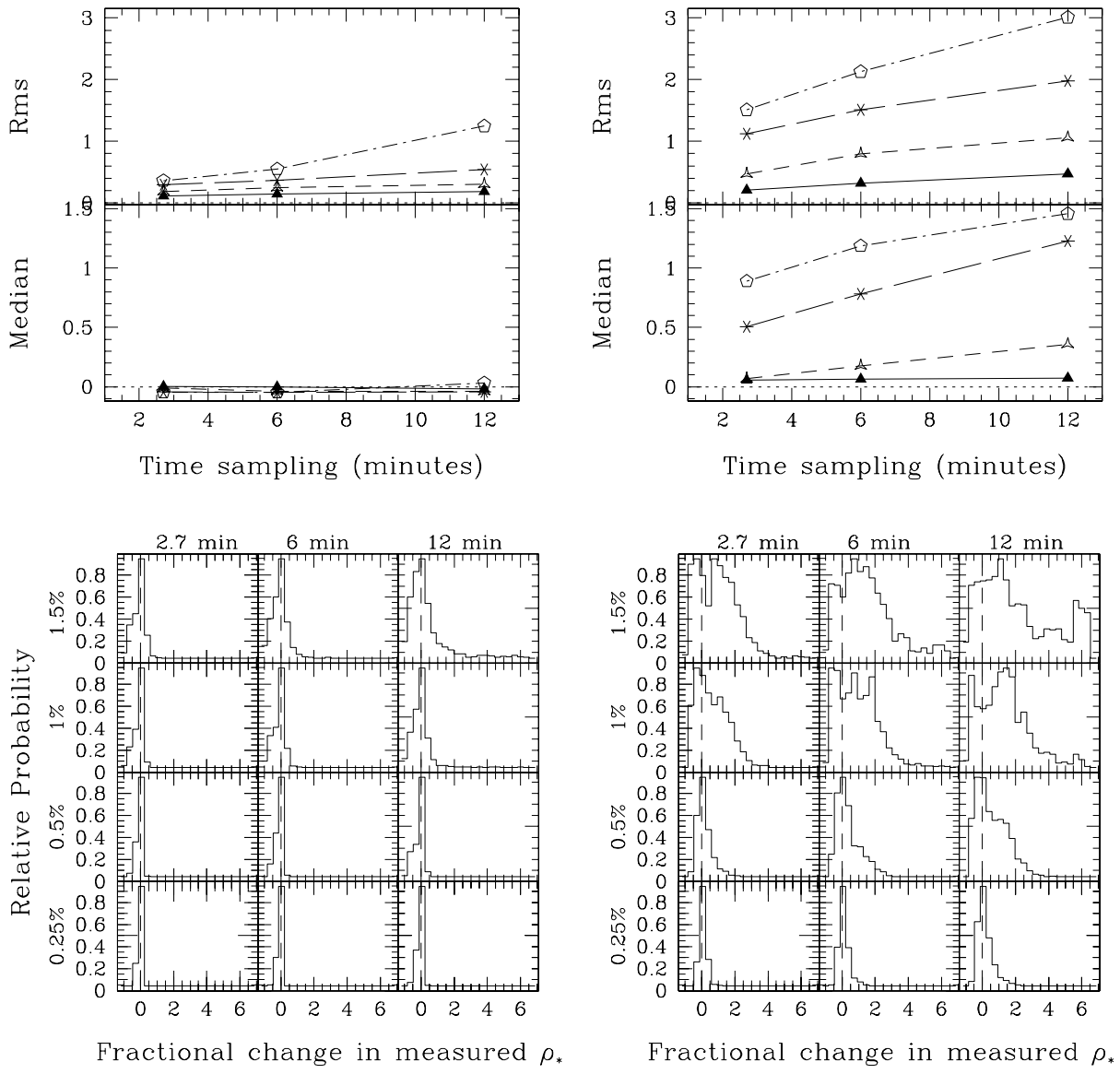

FIG. 5.—Fractional errors in the derived stellar density. See legend of Fig. 4 for details. Notice that for low photometric precision and time sampling the density is significantly overestimated for the $b = 0.7$ case. This is a consequence of the underestimate of b (see Fig. 4).

The stellar type (and hence R_* and R_p) may not be identified with 100% certainty from ρ_* alone as a result of confusion with stars slightly evolved off of the main sequence; the unique density derivation clearly does not specify the actual stellar mass and radius. As main-sequence stars begin to leave the main sequence, they will evolve with constant mass to lower density as their radius increases (on vertical downward lines in Fig. 7). These slightly evolved stars will fill in the box in Figure 7 to the lower left of the main-sequence star diagonal line. Nevertheless, for a given ρ_* the corresponding R_* of a main-sequence star will always be the upper limit of R_*, whether or not the star is slightly evolved. Thus, we can always determine an upper limit to R_*—and hence to R_p—from ρ_* alone. Furthermore, a lower limit to R_* for a given ρ_* can be derived with the consideration that stars with $M_* < 0.8\ M_\odot$ do not leave the main sequence in a Hubble time. Note that for densities corresponding to F0 V–M0 V stars, the largest error in the radius estimation will occur for an evolved $0.8\ M_\odot$ star with the density of an F0 V star; in this extreme scenario, the radius overestimate of the evolved star is only 25%. Beyond using the light curve alone, a derived surface gravity from a spectrum (measured to $\lesssim$20% precision for non–metal-poor stars near the main sequence; Allende Prieto et al. 1999) can be used with ρ_* derived from the transit light curve to determine M_* and R_*. Note that highly evolved stars will never be confused with main-sequence or slightly evolved stars, since ρ_* will be significantly lower for highly evolved stars.

The errors for ρ_* are described in § 4 and plotted in Figure 5. Figure 7 shows a plot of density versus main-sequence spectral type, together with reference error bars. With an error in t_F and t_T of less than 5 minutes and errors in ΔF of less than 1%, the stellar density can be constrained to 10%–20% depending on the transit shape (see § 4). A consequence of the unique solution of ρ_* is that transit fitting codes that find equally good fits for different combinations of M_* and R_* actually find *the same* ρ_* for these best fits.

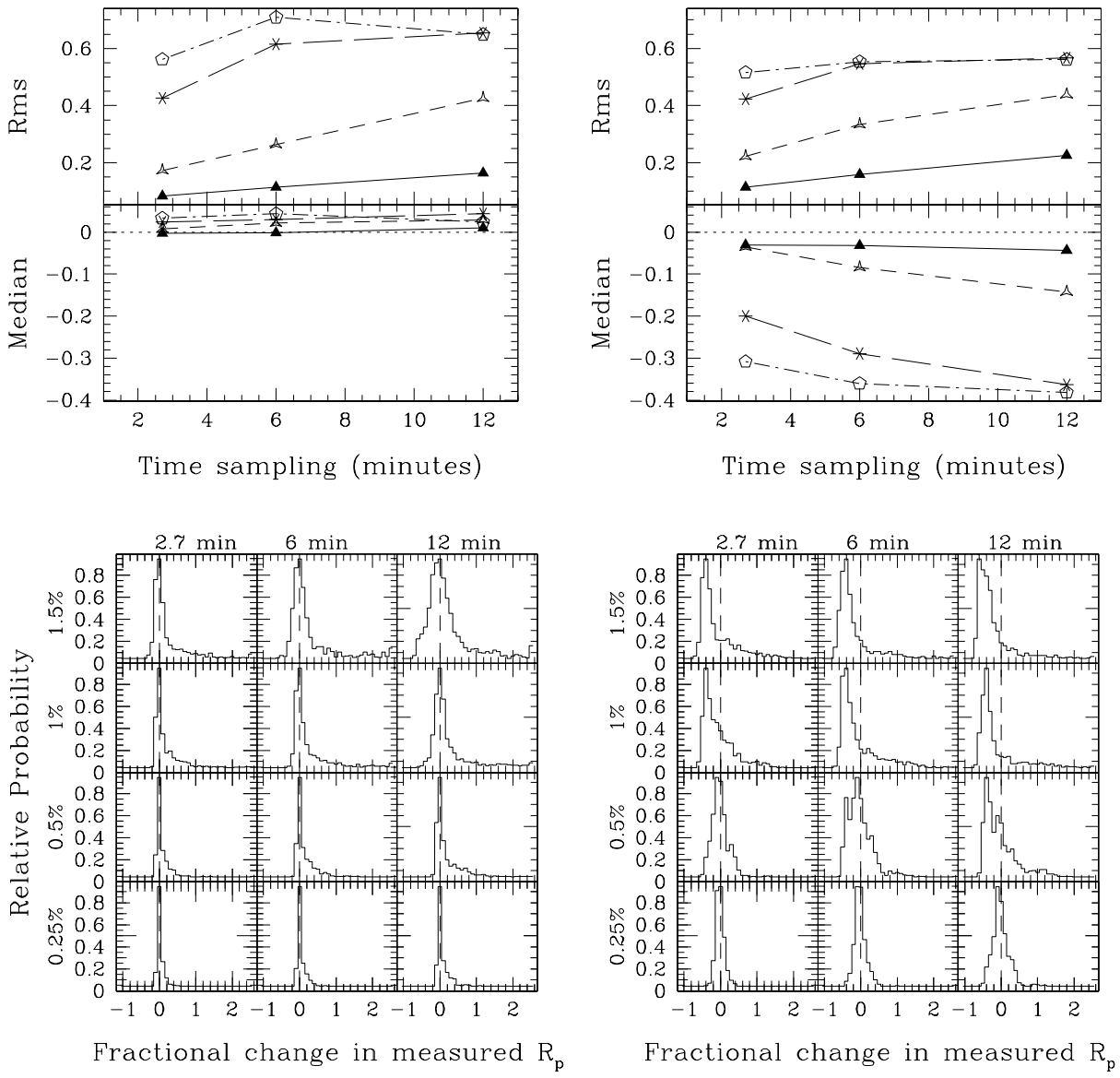

FIG. 6.—Fractional errors in the derived planet radius. See legend of Fig. 4 for details. Notice that for low photometric precision and time sampling the planet radius is consistently underestimated for the $b = 0.7$ case. This is a consequence of the underestimate of b (see Fig. 4). This underestimate will result in some M dwarfs being classified as planet-sized when using data with low photometric precision and time sampling.

5.2. *Contamination from Blended Stars: Transit Light Curve Alone*

The five-parameter solution to a planet transit light curve with two or more transits is not unique if there is additional light from a blended star (or indeed if any of the assumptions in § 2 are not fulfilled). A planet transit light curve can be mimicked by a stellar binary eclipsing system with contaminating light from a third, fully blended star. This contaminating light may come from an additional star physically associated by the eclipsing system (i.e., making a triple system), or by a chance alignment of a foreground or background star. The additional light from the blended star causes an otherwise deep eclipse to appear shallow and hence to mimic a planet transit light curve, as shown in Figure 8. This confusion is possible only when the eclipsing system has a flat-bottomed light curve, meaning that the eclipsing companion is fully superimposed on its primary star. Hereafter we call the eclipsing system plus the third fully blended star a "blend."

5.2.1. *Star-Planet Parameters and Blends*

The true, or actual, star-planet parameters will be confused by the contamination of blended light from an additional star. For selecting planet candidates for radial velocity follow-up it is useful to consider how some of the derived star and planet parameters change in the presence of blended light. In the following discussion we compare star and planet parameters naively derived from a transit light curve assuming no blend against those parameters derived by assuming the maximum possible amount of blended light.

The maximum amount of blended light for a given ΔF is computed by considering the largest possible companion consistent with a given ingress/egress duration. This is equivalent to assuming a central transit (i.e., $b = 0$) and computing the maximum

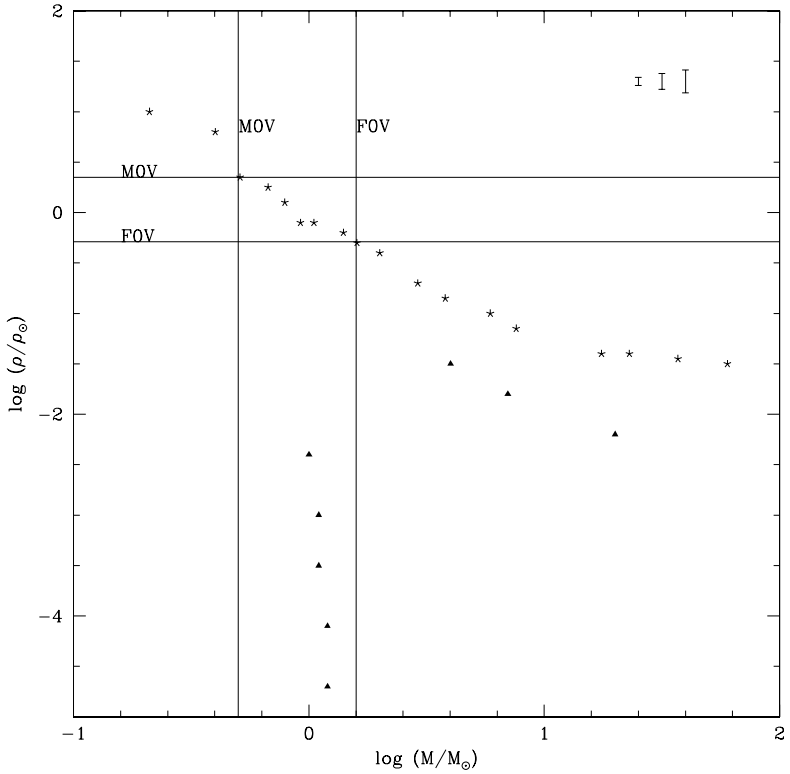

FIG. 7.—Stellar density ρ_* vs. star mass M_*. The asterisks show main-sequence stars, and the triangles show giant stars (Cox 2000). The unique solution of ρ_* from the planet transit light curves will give a position on the y-axis. The box M0 V–F0 V shows the main-sequence stars that are most appropriate for finding transiting planets. These stars have a very different density from giant stars and are therefore easily identifiable by their density alone. Although stars that have slightly evolved off of the main sequence will also populate the M0 V/F0 V box, their radii can still be estimated to $\lesssim$25% accuracy (see text). The error bars in the upper right corner are for fractional errors in ρ_* of 0.1, 0.2, and 0.3. See Fig. 5 for the errors in ρ_*.

ΔF possible for that given ingress/egress (i.e., t_F/t_T). Specifically, using $b = 0$ in equation (15),

$$\Delta F_{b,\mathrm{real}} \leq \Delta F_{b,\mathrm{real,max}} = \frac{(1 - t_F/t_T)^2}{(1 + t_F/t_T)^2} \ . \tag{21}$$

Here the subscript b refers to a blend; the subscript "obs" refers to the eclipsing system parameters derived ignoring the presence of the third fully blended star, whereas the subscript "real" refers to the actual parameters of the eclipsing binary. The subscript "max" refers to the quantities for the case of maximum possible blend (defined for a given t_F/t_T). $\Delta F_{b,\mathrm{obs}}$ is the eclipse depth as taken from the observed light curve, and $\Delta F_{b,\mathrm{real}}$ is the actual eclipse depth (i.e., in the absence of the blended star). The ratio $\Delta F_{b,\mathrm{real,max}}/\Delta F_{b,\mathrm{obs}}$ is shown in Figure 9*a*.

It is useful to consider the maximum difference between the density derived from a transit light curve in the presence of a blend ($\rho_{b,\mathrm{obs}}$) and the actual density of the eclipsed star ($\rho_{b,\mathrm{real}}$). We do this by using the simplified equation for ρ_*, equation (19), to compute the ratio $\rho_{b,\mathrm{obs}}/\rho_{b,\mathrm{real,max}}$:

$$1 \leq \frac{\rho_{b,\mathrm{real}}}{\rho_{b,\mathrm{obs}}} \leq \frac{\rho_{b,\mathrm{real,max}}}{\rho_{b,\mathrm{obs}}} = \left(\frac{\Delta F_{b,\mathrm{real,max}}}{\Delta F_{b,\mathrm{obs}}}\right)^{3/4} \ . \tag{22}$$

The stellar density is always underestimated from the light curve if a blend is present and ignored. A comparison of $\rho_{b,\mathrm{real,max}}$ and $\rho_{b,\mathrm{obs}}$ is shown in Figure 9*b* and is used in an application in § 5.3.

We can explore how the planet radius is affected by blends by considering how ρ_* is affected by blends (eq. [22]) together with the simplified solution for planet radius, equation (14). The actual radius of the eclipsing companion, $R_{p,b,\mathrm{real}}$, is related to the radius naively derived from the transit light curve ignoring the presence of a blend, $R_{p,b,\mathrm{obs}}$, by

$$\frac{R_{p,b,\mathrm{real}}}{R_{p,b,\mathrm{obs}}} = \left(\frac{\Delta F_{b,\mathrm{real}}}{\Delta F_{b,\mathrm{obs}}}\right)^{(3x-2)/(12x-4)} \leq \left(\frac{\Delta F_{b,\mathrm{real,max}}}{\Delta F_{b,\mathrm{obs}}}\right)^{(3x-2)/(12x-4)} \ , \tag{23}$$

where x is the exponent in the stellar mass-radius relation (eq. [5]). For main-sequence stars, $x \approx 0.8$ (Cox 2000) and the exponent in equation (23) becomes 0.071, so $R_{p,b,\mathrm{real}}/R_{p,b,\mathrm{obs}}$ is mildly dependent on the amount of blended light present. The fact that there is a maximum value for $\Delta F_{b,\mathrm{real}}$ together with equation (23) implies that $R_{p,b,\mathrm{real}}$ also has a maximum for a given t_F/t_T and ΔF. Figure 9*c* shows $R_{p,b,\mathrm{real,max}}/R_{p,b,\mathrm{obs}}$ as a function of transit shape parameterized by t_F/t_T. In the presence of a

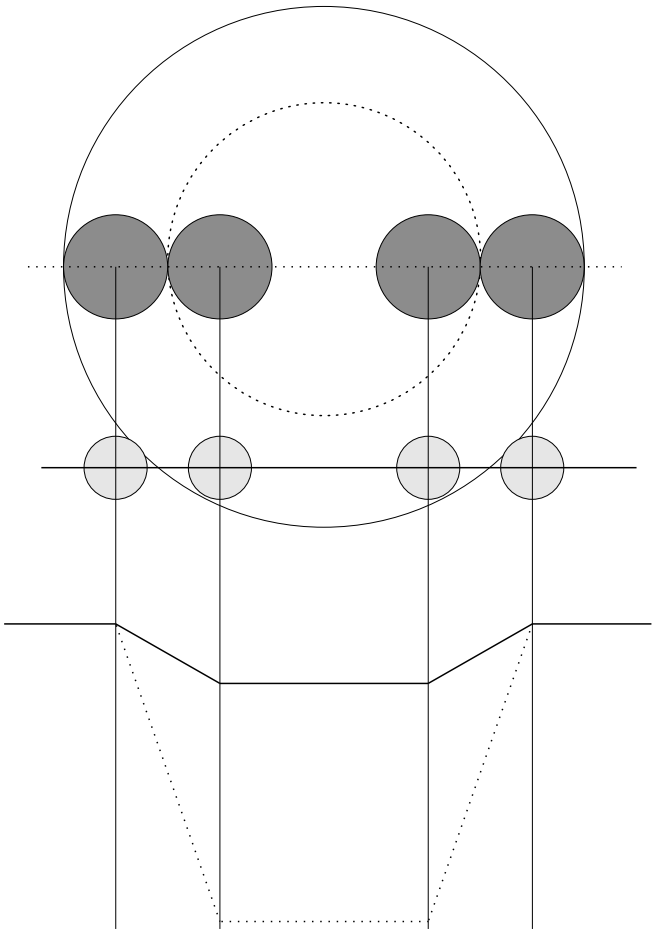

FIG. 8.—Effect of a blended star on a transit light curve. A schematic light curve (*dotted line at the bottom*) shows a relatively deep eclipse due to an eclipsing binary star system in which a small star centrally crosses the smaller primary star (*dotted circle*). In the presence of additional light from a third blended star (not shown), this deep eclipse will appear shallower, as shown by the solid-line transit curve. This shallower solid-line transit looks the same as a planet transit crossing a larger star (*solid circle*) with high impact parameter. Thus, there is no longer a unique solution to a transiting system in the presence of a blend. Note that any such blended transit will never look box-shaped, since the long ingress and egress are caused by the relatively long time it takes for the secondary star to cross the limb of the primary star.

blend, the actual radius of the eclipsing companion is always larger than the radius derived from the eclipsing light curve. Thus, this figure shows the importance of ruling out blends: *the eclipsing companion in a blended case could be larger than expected for a close-in planet* ($R_p \sim R_J$) *by 20%–50%*.

5.2.2. *Probability of Blends and Blend Limits*

Transits with short ingress and egress times (box-shaped transits with large t_F/t_T) are least likely to be affected by blended stars and can be the best planet transit candidates for follow-up radial velocity mass measurements. There are two reasons for this. First, less blended light can be hidden in a shallow transit with large t_F/t_T than one with small t_F/t_T. This is seen directly from the maximum value of $\Delta F_{b,\mathrm{real,max}}$ given in equation (21) and shown in Figure 9*a*.

The second reason why box-shaped transits are least likely to be affected by blended stars is because of the geometric probability for different transit shapes given random orientations of orbital inclinations.

First, it is useful to recognize that the unique solution to the planet-star parameters is in part possible because for a given ΔF there is a one-to-one correspondence between the impact parameter b and the transit shape as parameterized by t_F/t_T. This b-versus-t_F/t_T relation is nonlinear, as shown in Figure 3. For a random orientation of orbital inclinations, the cumulative probability P_c that an unblended transit will have impact parameter b *smaller* than some given value b_x is proportional to b_x; the maximum value of b for a transit is $1 - R_p/R_* = 1 - (\Delta F)^{1/2}$, where $(\Delta F)^{1/2}$ is the value for an unblended transit. Thus, the cumulative probability that an unblended transit will have b *larger* than b_x is described by

$$P_c(b \leq b_x) = \frac{1 - \sqrt{\Delta F} - b_x}{1 - \sqrt{\Delta F}} \tag{24}$$

and is shown in Figure 10*a*. Because of the one-to-one correspondence between b and transit shape, we can also express the cumulative probability in terms of t_F/t_T (i.e., transit shape), shown in Figure 10*b*. The cumulative probability in equation (24) and Figure 10 can be used to show that for an ensemble of transits, there should be more "box-shaped" transits (large t_f/t_T)

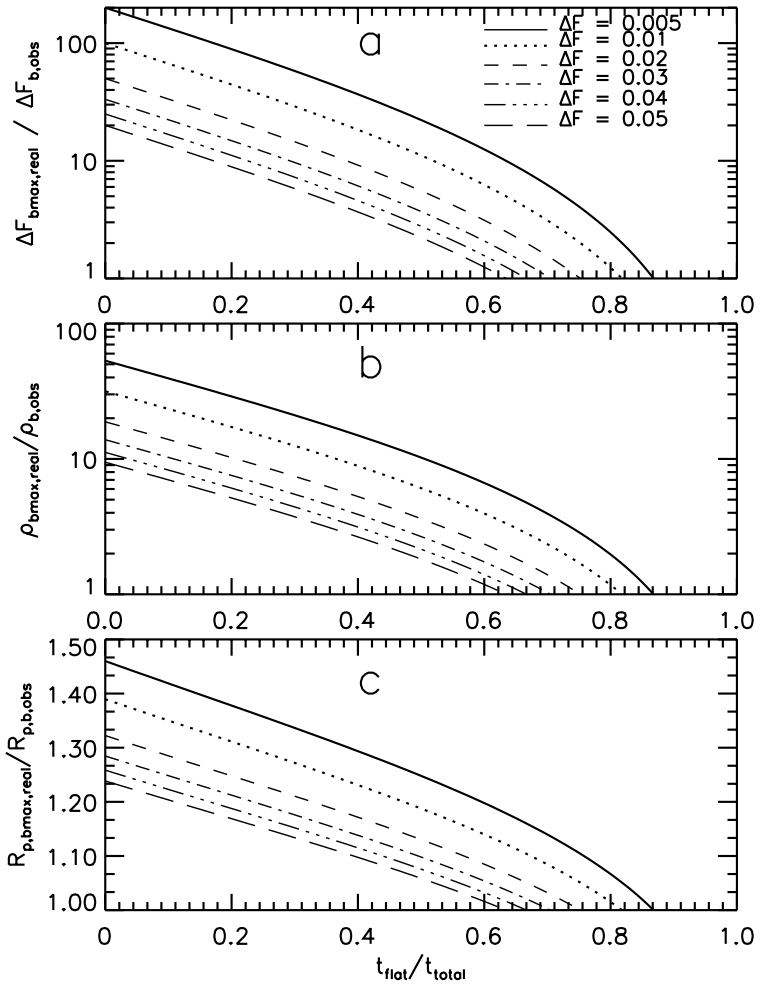

FIG. 9.—Maximum effect of a third fully blended star on the naively derived eclipsing system's parameters ΔF, ρ_*, and R_p. (*a*) Ratio between the maximum real eclipse depth in the presence of a blend $\Delta F_{b,\mathrm{real,max}}$ and the observed eclipse depth $\Delta F_{b,\mathrm{obs}}$ as a function of transit shape parameterized by t_F/t_T (see eq. [21]). For a small transit depth (e.g., $\Delta F = 0.005$) and a small t_F/t_T (i.e., a nearly triangular transit shape) a large amount of extra light can be hidden in the transit light curve. (*b*) Ratio between the maximum real stellar density $\rho_{b,\mathrm{real,max}}$ and the naively derived density $\rho_{b,\mathrm{obs}}$ in the case of a blend. This ratio depends on both t_F/t_T and ΔF (eqs. [22] and [21]). Note that the real stellar density is always higher than the "observed" stellar density naively derived from a light curve ignoring the blend. (*c*) Ratio between the maximum real companion radius $R_{p,b,\mathrm{real,max}}$ in the presence of a blend and the naively derived radius $R_{p,b,\mathrm{obs}}$, assuming the mass-radius relation for main-sequence stars (see eq. [23]). Note that in the case of a blend, the real eclipse depth, real stellar density, and real companion radius are always larger than the naively derived observed values.

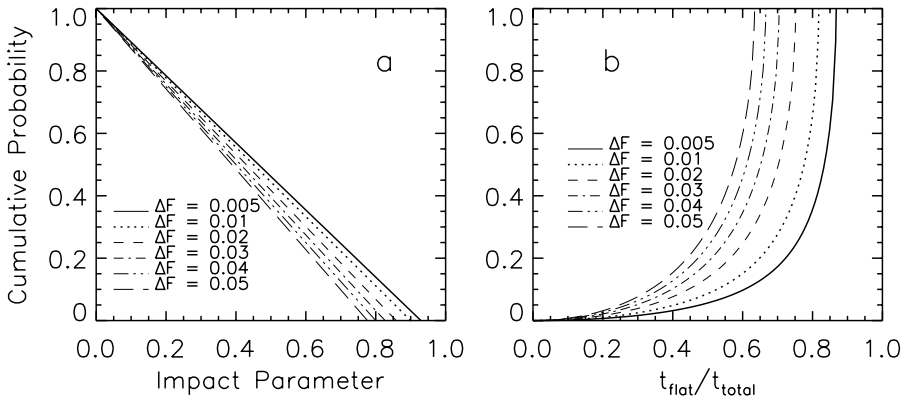

FIG. 10.—(*a*) Cumulative probability (P_c) that, for a random orientation of orbital inclinations, a transit has impact parameter b that is *larger* than a specified impact parameter b_x (shown on the x-axis). This cumulative probability is just due to geometry. (*b*) Same cumulative probability as a function of transit shape, as parameterized by t_F/t_T. P_c can be described by both b and t_F/t_T because there is a one-to-one correspondence between them for a given transit depth, as shown in Fig. 3. The P_c shows that "boxlike" transit shapes (i.e., high t_F/t_T) are much more common than transits with long ingress and egress (i.e., transits with small t_F/t_T). If in a transit survey a large fraction of transits of a given ΔF are found to have small t_F/t_T, this is an indication that most of these systems are likely blended (see Fig. 8).

than transits with very long ingress/egress times (small t_F/t_T).

The signal-to-noise ratio that must be reached to be able to completely rule out a possible blend can be determined from the maximum real eclipse depth $\Delta F_{b,\mathrm{real,max}}$. The light from the eclipsing primary star is always less than or equal to the total amount of light from the blended system and has a minimum value given by the maximum blend:

$$1 \geq \frac{F_{\mathrm{primary}}}{F_{b,\mathrm{total}}} = \frac{\Delta F_{b,\mathrm{obs}}}{\Delta F_{b,\mathrm{real}}} \geq \frac{\Delta F_{b,\mathrm{obs}}}{\Delta F_{b,\mathrm{real,max}}} \ . \tag{25}$$

Thus, the quantity $\Delta F_{b,\mathrm{obs}}/\Delta F_{b,\mathrm{real,max}}$ gives a lower limit to the fraction of the observed light that comes from the primary star in the eclipsing system. This can be used to establish the data quality necessary to find or rule out a blend in a given case. The light from the eclipsing primary in the blend could be detected, for example, by cross-correlating spectra of the blend with a suite of stellar templates to see if two cross-correlation peaks are present, or by resolving the blend with high spatial resolution imaging (e.g., from space or adaptive optics).

We summarize this subsection as follows:

1. Box-shaped transits are the best planet candidates for radial velocity mass follow-up because (1) the least amount of blended light can be hidden in box-shaped transits and (2) for an ensemble of randomly oriented orbital inclinations there should be many more box-shaped transits (i.e., with large t_F/t_T) than transits that have a very sloped ingress and egress (i.e., with small t_F/t_T). See Figure 1.
2. In the presence of a blended star, the real planet radius is always larger than the naively derived planet radius ignoring the blend.
3. The maximum brightness of a possible contaminating star can be derived from the transit light curve.

5.3. *Contamination from Blended Stars: Transit Light Curve and a Known Spectral Type*

Knowing the spectral type independently of the parameters derived from the transit light curve can be extremely useful in ruling out blends. With M_* and R_* determined from a spectral type, the system of equations (1)–(4) is overconstrained. If the stellar density $\rho_{b,\mathrm{obs}}$ as derived from the light curve from equation (9) is very different from the density ρ_{spect} of the observed spectral type, then something is amiss with the light-curve assumptions in § 2. A possibility is the case of a blended star discussed above. Thus, comparing ρ_{obs} with ρ_{spect} is extremely useful for detecting the presence of a blend.

For example, the density can be overestimated by a factor of up to 10 for $t_F/t_T = 0.4$ and $\Delta F = 0.1$. The maximum density ratios on Figure 9*b* can be compared directly with the actual stellar main-sequence densities shown in Figure 7. Furthermore, by comparing ρ_{obs} and ρ_{spect}, we can detect the presence of a blend to a lower limit determined by the fractional errors in the stellar density, $\delta\rho_*/\rho_* \simeq [(\delta\rho_{\mathrm{obs}}/\rho_{\mathrm{obs}})^2 + (\delta\rho_{\mathrm{spect}}/\rho_{\mathrm{spect}})^2]^{1/2}$. From equations (25) and (22) we can see that it will be possible to detect blends with $F_{\mathrm{primary}}/F_{b,\mathrm{total}} = \Delta F_{b,\mathrm{obs}}/\Delta F_{b,\mathrm{real}} \lesssim (1 - \delta\rho_*/\rho_*)^{4/3}$. Note that the error in ρ_{spect} must account for the fact that the spectrum may be dominated by the blended star, rather than by the primary star in the eclipsing system.

5.4. *Blends and Statistics*

Blended stars may be a common contaminant in transit searches (D. Latham 2001, private communication; G. Mallén-Ornelas et al. 2003, in preparation) as a result of either very wide binaries or, less likely in an uncrowded field, a chance alignment of a foreground or a background field star. In the presence of a third fully blended star some planet transits will be "washed out" and not detectable. Hence, it is important to know the blend frequency to determine the frequency of transiting planets. Even without a measured stellar spectral type, the frequency of blends contaminating the sample of planet candidates can be determined statistically by considering all of the flat-bottomed eclipses of various depths in the following way. Assuming that the orbital inclination distribution is uniform, for a given ΔF light curves should have a certain distribution of t_F/t_T (see the probability discussion in § 5.2). Deviations from each expected distribution can be explained by eclipses being made more shallow than they should be by contaminating blended stars. The fraction of blended stars will also allow a statistical estimate of how many transits may be missed as a result of blends.

5.5. *Period Derivation from Single-Transit Light Curves and a Known Spectral Type*

The period can be estimated for a light curve with only one transit if M_* and R_* are known from a measured spectral type. Again, this is because the system of equations (1)–(4) that describe the transit light curve is overconstrained when M_* and R_* are known. Considering that M_* and R_* are known and that the impact parameter is derived from equation (7), the period can be solved for from the following function of P:

$$\frac{4\pi^2}{P^2 G}\left\{\frac{(1+\sqrt{\Delta F})^2 - b^2\left[1-\sin^2(t_T\pi/P)\right]}{\sin^2(t_T\pi/P)}\right\}^{3/2} = \frac{M_*}{R_*^3} \ , \tag{26}$$

where the right-hand side can be determined from the stellar spectral type. Under the approximation $t_T\pi/P \ll 1$, the period is simply given by

$$P = \frac{M_*}{R_*^3}\frac{G\pi}{32}\frac{\left(t_T^2 - t_F^2\right)^{3/2}}{\Delta F^{3/4}} \ . \tag{27}$$

For P in days, the first term on the right-hand side is $G\pi/32 = 288.73$. The error for this P estimate is not easily derived because the errors in t_F and t_T are highly non-Gaussian and are often correlated. The fractional error in the period, $\delta P/P$, can be estimated for small errors in time sampling and photometric precision by noting that equation (27) is derived from the implified equation for ρ_* (eq. [19]) and that M_* and R_* would be known from the spectral type: $\delta P/P = [(\delta\rho_{\rm obs}/\rho_{\rm obs})^2 + (\delta\rho_{\rm spect}/\rho_{\rm spect})^2]^{1/2}$, where $\delta\rho_{\rm obs}/\rho_{\rm obs}$ is the fractional error in ρ_* derived from the transit light curve and $\delta\rho_{\rm spect}/\rho_{\rm spect}$ is the fractional error in ρ_* derived from the spectral type. Thus, following the discussion in § 4 and assuming $\delta\rho_{\rm spect}/\rho_{\rm spect} \lesssim 0.1$, the period can be determined to $\sim$15%–20% (depending on transit shape) for $\delta t < 5$ minutes and $\sigma \sim 0.0025$ mag.

An upper limit to the period can be estimated even without knowing t_F,

$$P \leq \frac{G\pi}{32}\frac{M_*}{R_*^3}\frac{t_T^2}{\Delta F^{3/4}} \ . \tag{28}$$

This upper limit is valid even in the case of a blend where $\Delta F_{b,\rm real}$ is larger than the observed ΔF.

6. LIMB DARKENING

So far we have described the non–limb-darkened analytical solution for planet and star parameters from the extrasolar planet transit light curve and used the analytical solution to explore the behavioral trends of the derived parameters. For example, we have found that the stellar density can be determined from the light curve alone. Moreover, we have used the analytic solution to explore the parameter dependencies of false positive transit signals such as blends. Once candidates are found with the quick parameter estimate, they should be fitted with appropriate limb-darkened models in order to determine more accurate star and planet parameters (e.g., Mandel & Agol 2002). We have so far ignored limb darkening because limb darkening would have complicated the very useful analytical explorations. It is still important to determine the effect of ignoring limb darkening on the derived parameters. In this section we describe the effects of limb darkening on planet light curves, on derived parameters, and on the applications of the unique solution described in § 5.

Light curves taken in a bandpass blueward of $\sim$1 μm for solar-like stars show noticeable limb darkening. The general effect of limb darkening is to (1) change the depth of the light curve ΔF as a function of impact parameter (making the light curve deeper for most values of impact parameter), (2) make the flat bottom rounder (and hence the "flat part" shorter, thus reducing t_F), and (3) blur the boundary between ingress/egress and the flat bottom. These effects are shown in Figure 11.

It is possible to incorporate limb darkening into the mathematical description of a planet transit light curve by parameterizing the transit shape by the slope of the ingress/egress instead of by t_F and t_T. The ingress/egress slope is mainly dependent on the time it takes the planet to cross the stellar limb but is also affected by limb darkening. The transit depth ΔF is also dependent on limb darkening and orbital inclination. A unique solution still exists when limb darkening is included; however, the equations that describe the limb-darkened transit light curve take a cumbersome form, and there is no longer a simple analytical solution. Note that in practice the work described in this paper requires that limb darkening is weak. In particular, it is essential to be able to distinguish a flat bottom in the eclipses to be able to rule out contaminating grazing binaries and other partial stellar eclipses. *I*-band eclipses are good enough to distinguish flat bottoms, as shown from real data from the EXPLORE transit search (Mallén-Ornelas et al. 2003). For noisy data taken in bluer bandpasses, however, partial eclipses would no longer be clearly distinguishable from flat-bottomed transits.

To assess the effects of ignoring limb darkening, we have made a simulation that generates model light curves with solar limb darkening at several wavelengths (4500 Å, 5500 Å, 8000 Å, and 3 μm). The limb-darkening parameters are from Cox (2000). We have used $P = 3$ days, $M_* = 1\ M_\odot$, $R_* = 1\ R_\odot$, 2% eclipse depth, 2.7 minute time sampling, 1% noise, and $0 \leq b \leq 0.8$. We have then fitted 1000 limb-darkened simulated light curves with a model light curve that has no limb darkening.

Figure 12 shows the results of our simulations' three important parameters: b, ρ_*, and R_p. The left-hand panels of Figure 12 show the mean deviation between input parameters and those found by the non–limb-darkened fit, as a function of impact parameter of the input transit. This approximates the effect of trying to parameterize a real limb-darkened eclipse by single values of t_T, t_F, and ΔF. The impact parameter b is the parameter that is most affected by neglecting limb darkening. Specifically, since limb darkening makes t_F seem smaller, the impact parameter gets overestimated; this is particularly noticeable for nearly central transits with small impact parameters. In turn, the overestimate of b causes an underestimate of ρ_* and an overestimate of R_p. These biases are very similar for simulations with 0.25% and 0.5% noise, since they are due to the mismatch in the shape of transits with and without limb darkening, rather than to the noise in the light curve. The right-hand panels of Figure 12 show the same median deviation between input parameters and a fit with the appropriate limb-darkened model. These panels show that color-dependent biases are negligible when the correct limb darkening is chosen for the model (the small biases present are not a function of color and are due to the noise and finite time sampling in the light curve, as shown in § 4).

We are most interested in errors in the *I* band where limb darkening is weak. For the *I* band, ρ_* can be underestimated by up to 30% depending on the actual impact parameter of the transit. For *I*-band light curves the planet radius can be overestimated by up to 30%. These errors for *I* band are not much larger than random errors in the fit as a result of the photometric noise and finite time sampling in light curves (see our simulations in § 4; Figs. 4, 5, and 6).

None of the applications of the unique solution (§ 5) are adversely affected by ignoring limb darkening in the *I* band. (1) The difference in ρ_* between a main-sequence star and a giant star is much larger than the 30% bias in ρ_* as a result of ignoring limb darkening. (2) For a quick estimate of the planet radius a bias of 30% is significant, but the bias is small enough so that it is still possible to determine whether the light curve is worth a more detailed fit based on the companion size. (3) The impact parameter b is used for assessing whether a light curve is contaminated by a blended star. A blend causes a derivation of an extremely

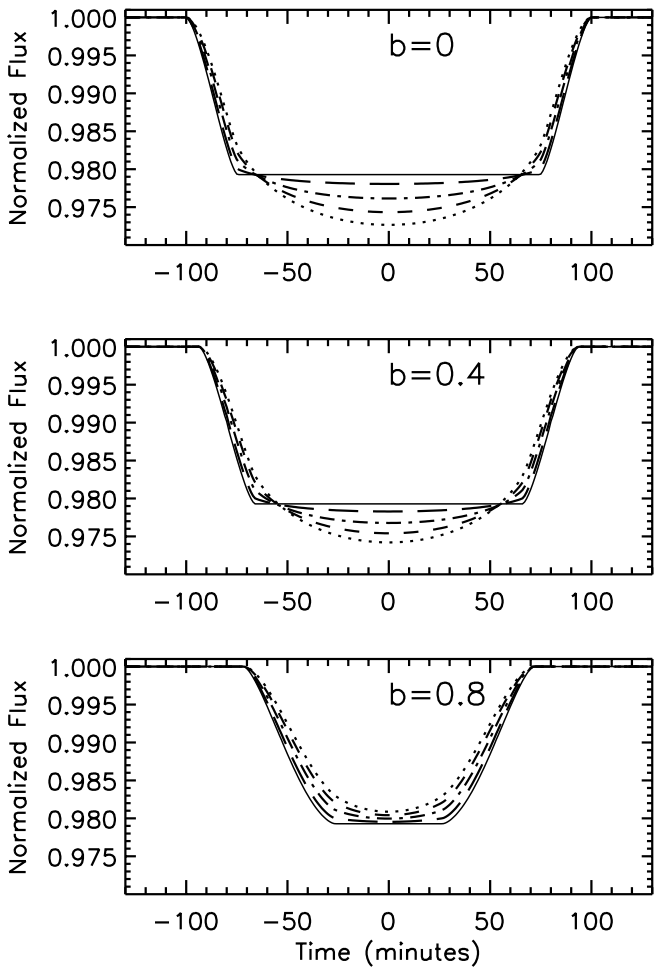

FIG. 11.—Solar limb-darkening dependence of a planet transit light curve. The limb-darkening parameters are from Cox (2000). In these theoretical light curves the planet has $R_p = 1.4\ R_J$ and $a = 0.05$ AU and the star has $R_* = R_\odot$ and $M_* = M_\odot$. The solid curve shows a transit light curve with limb darkening neglected. The other planet transit light curves have solar limb darkening at wavelengths 3, 0.8, 0.55, and 0.45 μm. From top to bottom the panels show transits with different impact parameters b, which correspond to inclinations $\cos i = bR_*/a$.

high b close to the maximum possible for a full eclipse. While the biases due to ignoring limb darkening increase b most significantly for small values of b, in general the biases do not increase b to the extremely large values typical of blended eclipses.

In summary, if a limb-darkened light curve is fitted with a non–limb-darkened model, systematic biases arise (shown in Fig. 12). The limb-darkening error is intrinsic to the difference in shape of transits with and without limb darkening and will always be roughly the same for limb darkening of different photometric precision. Importantly, with a fit with the proper limb-darkening parameters, there are no color-dependent biases due to limb darkening.

7. SUMMARY

We have presented the equations that describe a light curve with two or more transits and have presented the unique solution for the impact parameter b, the ratio of the orbital semimajor axis to stellar radius a/R_*, and stellar density ρ_*. Furthermore, with the stellar mass-radius relation we can uniquely derive the five parameters M_*, R_*, i, a, and R_p. This unique solution is only possible under the assumptions listed in § 2, most importantly that the light curve is from a single star (i.e., not two or more fully blended stars), that the planet is dark and is in a circular orbit, and that the light-curve transits have flat bottoms (which can be obtained at red or longer wavelengths).

We have found the following:

1. A simple analytical solution that can be used to quickly estimate the planet-star parameters, most importantly ρ_* and R_p (see eqs. [9], [14], and [19]).
2. The stellar density can be uniquely determined from the transit light curve alone. Fitting codes that solve for star-planet parameters will find a number of best fits for different combinations of M_* and R_*; these best fits will have the same stellar density.
3. For noisy data, the impact parameter b, R_*, and R_p are underestimated and ρ_* is overestimated as a result of a nonlinear one-to-one correspondence for a given ΔF between b and transit shape (as parameterized by t_F/t_T).

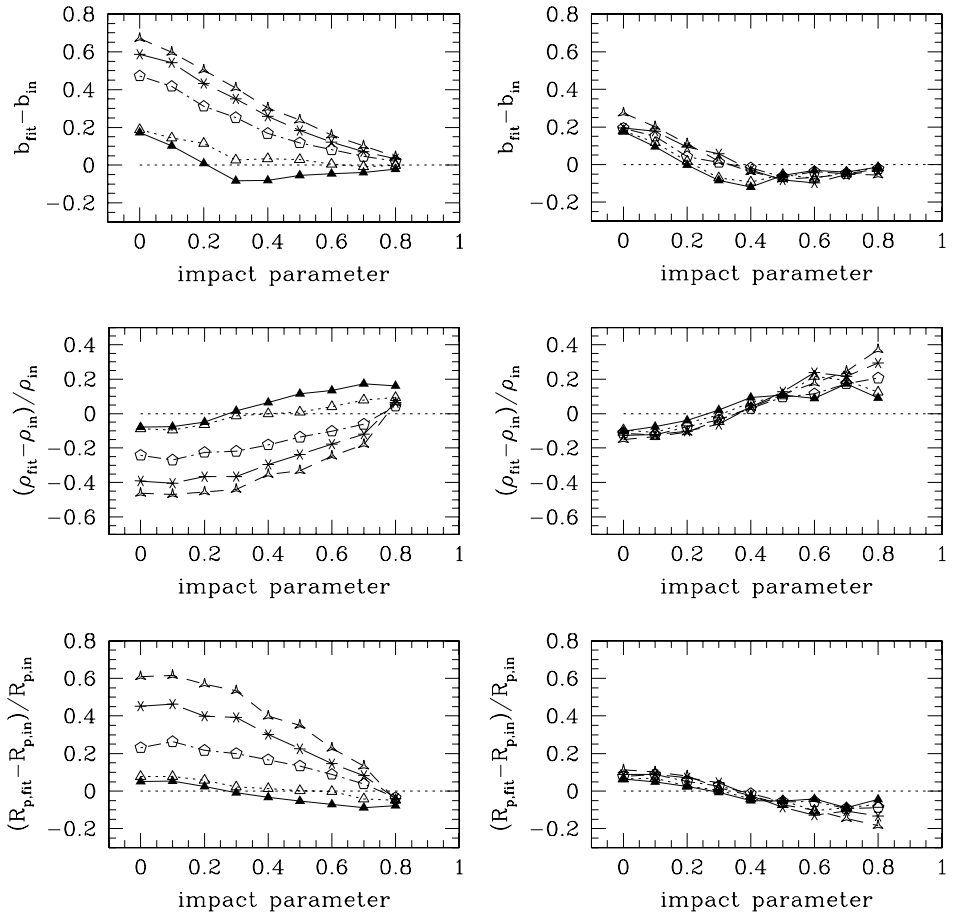

FIG. 12.—Comparison of fits with and without limb darkening. Shown are the *median* values of the difference between the fit parameters (X_{fit}) and the input model parameters (X_{in}), as a function of input impact parameter. The fits were performed for 1000 input model light curves that had 2.7 minute time sampling, 1% rms photometric noise, and solar limb darkening for a range of bandpasses (with limb-darkening coefficients from Cox 2000). While all the input light curves have limb darkening, the left-hand panels show the results of fits for a model that has no limb darkening, thus approximating the effect of ignoring limb darkening in the analytic solution. As a comparison, the right-hand panels show results for fits with a model that has limb darkening for the appropriate color. Open triangles correspond to 0.45 μm input model light curves, asterisks to 0.55 μm, pentagons to 0.8 μm (closely approximating the *I* band), open triangles to 3 μm, and filled triangles to no limb darkening. While there are biases in the median fit parameters when limb darkening is ignored, color-dependent biases are negligible when light curves are fitted with a model that has the appropriate limb-darkening parameterization. The main point of this figure is that errors for the *I* band are not much larger than random errors in the fit due to the photometric noise and finite time sampling in light curves.

The existence of the unique solution for the above parameters allows several interesting applications, including the following:

1. The stellar radius and the planet radius can be estimated based on ρ_*.
2. The likelihood that a shallow transit is due to contamination from a fully blended star can be estimated, with box-shaped transits being the least likely to be contaminated by blends.
3. A comparison of ρ_* as determined from the transit light curve with ρ_* from a spectral type can help identify blended stars and hence indicate that shallow eclipses are not due to planet transits.
4. In the presence of a blend the actual eclipsing companion radius is always larger than the radius derived from the light curve.
5. The period from a single transit event can be estimated with a known spectral type.

For most of the above applications time sampling of $\delta t \lesssim 5$ minutes and photometric precision of $\sigma \lesssim 0.005$ mag are needed (or more generally $\sigma^2 \delta t \lesssim 1.5 \times 10^{-4}$ mag^2 minutes). These values are for a two-transit light curve; multiple low–time-sampled transit light curves can be folded for higher effective time sampling and are useful as long as the photometric precision is high enough. These values of time sampling and photometric precision are reachable with current planet transit surveys (e.g., Mallén-Ornelas et al. 2003). The transit shape must be well defined by high photometric precision and high time sampling because most star-planet parameters depend on transit shape. Specifically, a limiting factor is time sampling of ingress and egress and their start and end times to determine transit shape.

We thank Howard Yee, Tim Brown, Scott Gaudi, and Gil Holder for useful discussions and Jean Schneider for useful comments. We thank the referee, Bill Hubbard, for a thoughtful reading of the manuscript and for useful suggestions. S. S. is supported by the W. M. Keck Foundation. S. S. thanks John Bahcall for valuable advice, generous support, and encouragement. G. M.-O. thanks John Bahcall and the IAS for generous hospitality during visits when this work was carried out.

REFERENCES

Allende Prieto, C., López, G., Ramón, J., Lambert, D. L., & Gustafsson, B. 1999, ApJ, 527, 879
Borucki, W. J., Caldwell, D., Koch, D. G., & Webster, L. D. 2001, PASP, 113, 439
Brown, T. M., Charbonneau, D., Gilliland, R. L., Noyes, R. W., & Burrows, A. 2001, ApJ, 552, 699
Charbonneau, D., Brown, T. M., Noyes, R. W., & Gilliland, R. L. 2002, ApJ, 568, 377
Cox, A. N. 2000, in Allen's Astrophysical Quantities (New York: AIP), 355–357
Guillot, T., & Showman, A. P. 2002, A&A, 385, 156
Jenkins, J. M., Caldwell, D. A., & Borucki, W. J. 2002, ApJ, 564, 495
Kopal, Z. 1979, The Language of the Stars (Dordrecht: Holland)
Mallén-Ornelas, G., Seager, S., Yee, H. K. C., Gladders, M. D., Brown, T. M., Minniti, D., Ellison, E., & Mallén-Fullerton, G. 2002, in ASP Conf. Ser., Scientific Frontiers in Research on Extrasolar Planets, ed. D. Demming & S. Seager (San Francisco: ASP), in press
Mallén-Ornelas, G., Seager, S., Yee, H. K. C., Minniti, D., Gladders, M. D., Mallén-Fullerton, G., & Brown, T. M. 2003, ApJ, 582, 1123
Mandel, K., & Agol, E. 2002, ApJ, 580, L171
Sackett, P. 1999, in Planets outside the Solar System: Theory and Observations, ed. J.-M. Mariotti & D. Alloin (Dordrecht: Kluwer), 189–227
Schneider, J., & Chevreton, M. 1990, A&A, 232, 251
Seager, S., & Hui, L. 2002, ApJ, 574, 1004
Udalski, A., Zebrun, K., Szymanski, M., Kubiak, M., Soszynski, I., Szewczyck, O., Wyrzykowski, L., & Pietrzynski, G. 2002a, Acta Astron., 52, 115
Udalski, A., et al. 2002b, Acta Astron., 52, 1
Yee, H. K. C., Mallén-Ornelas, G., Seager, S., Gladders, M. D., Brown, T., Minniti, D., Ellison, S. L., & Mallén-Fullerton, G. 2003, Proc. SPIE, in press
Zucker, S., & Mazeh, S. 2002, ApJ, 568, L113